Molecular Basis for the Cation Selectivity of *Salmonella typhimurium* Melibiose Permease

Satoshi Katsube [1], Ruibin Liang [2*], Anowarul Amin [1†], Parameswaran Hariharan [1] and Lan Guan [1*]

***1* - Department of Cell Physiology & Molecular Biophysics,** *Center for Membrane Protein Research, School of Medicine, Texas Tech University Health Sciences Center, Lubbock, TX 79430, United States*

***2* - Department of Chemistry and Biochemistry,** *Texas Tech University, Lubbock, TX 79409, United States*

Correspondence to Ruibin Liang and Lan Guan: *rliang@ttu.edu (R. Liang), Lan.Guan@ttuhsc.edu (L. Guan), @LiangRuibin (R. Liang)*

https://doi.org/10.1016/j.jmb.2022.167598

Edited by Nieng Yan

Abstract

Cation selectivity and coupling are important attributes of cation-coupled symporters. *Salmonella typhimurium* melibiose permease ($MelB_{St}$) catalyzes the co-transport of galactosides with cations (H^+, Li^+, or Na^+). 3-D crystal structures of $MelB_{St}$ have revealed the molecular recognition for sugar substrates, but the cation binding and coupling mechanisms have not been defined to atomic levels. In its human homolog MFSD2A, a lethal mutation was mapped at its Na^+-binding pocket; however, none of the structures in this subfamily resolved its cation binding. In this study, molecular dynamics simulations reveal the binding interactions of Na^+ and Li^+ with $MelB_{St}$. Interestingly, Thr121, the lethal mutation position in MFSD2A, forms stable interaction with Na^+ but is at a distance from Li^+. Most mutations among 11 single-site Thr121 mutants of $MelB_{St}$ exhibited little effects on the galactoside binding, but largely altered the cation selectivity with severe inhibitions on Na^+ binding. Few mutants (Pro and Ala) completely lost the Na^+ binding and Na^+-coupled transport, but their Li^+ or H^+ modes of activity were largely retained. It can be concluded that Thr121 is necessary for Na^+ binding, but not required for the binding of H^+ or Li^+, so a subset of the Na^+-binding pocket is enough for Li^+ binding. In addition, the protein stability for some mutants can be only retained in the presence of Li^+, but not by Na^+ due to the lack of affinity. This finding, together with other identified thermostable mutants, supports that the charge balance of the cation-binding site plays an important role in $MelB_{St}$ protein stability.

Introduction

The melibiose permease of *Salmonella typhimurium* ($MelB_{St}$) is a secondary active transporter catalyzing stochiometric symport of galactopyranosides with a Na^+, H^+ or Li^+.[1,2] MelB is a prototype of the major facilitator superfamily subgroup 2 (MFS_2)[3,4] among the largest MFS membrane transporters.[5,6] MelB homologs in human play important roles from lipid uptake such as the Na^+-dependent phospholipids transporter MFSD2A[7] to cancer development.[8,9] The high-resolution structures for $MelB_{St}$[3,10] were solved, and the structures for the eukaryotic homolog MFSD2A have been also resolved.[11,12] Structurally, MelB is composed of 12 transmembrane α-helices organized into two pseudo-symmetric bundles (Figure 1(a, b)). The outward-facing structures bound with α-nitrophenyl galactoside (α-NPG) or dodecyl melibioside (DDMB) showed that the sugar speci-

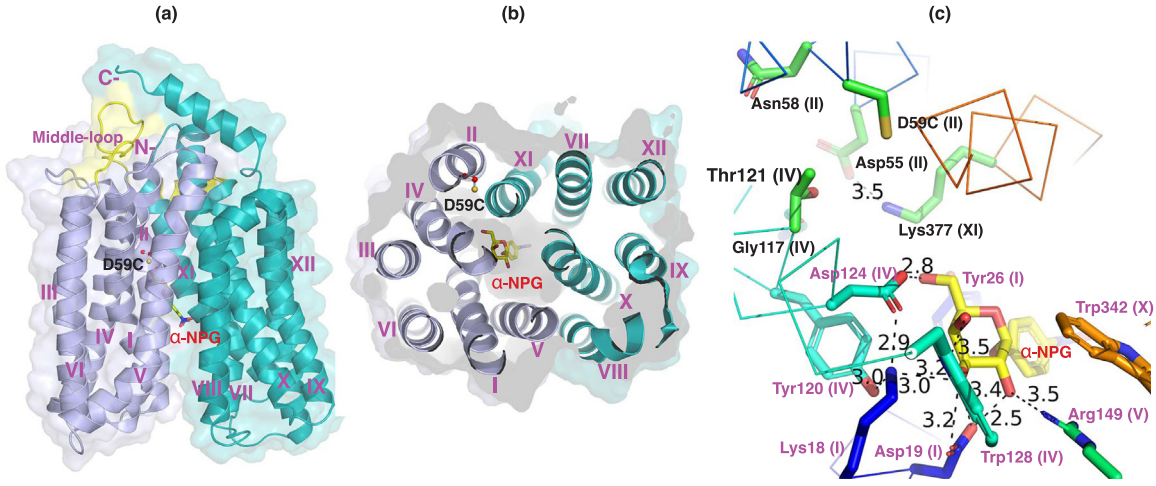

Figure 1. Sugar-bound outward-facing crystal structure of D59C MelB$_{St}$. (a) Overall fold and helical packing [PDB ID, 7L17]. A cartoon representation of the D59C MelB$_{St}$ structure bound with α-NPG is viewed parallel to the membrane, shown in cartoon representation colored in blue for N-terminal domain and in green for the C-terminal domain, and superimposed with a surface representation. The cytoplasmic middle loop is colored in yellow. Transmembrane helix is numbered in Roman numerals. The bound α-NPG is colored in yellow; the position Asp59 on helix II is shown in ball and stick. **(b)** Viewed from cytoplasmic side. **(c)** The galactoside binding and cation-binding pocket. The bound α-NPG molecule is colored in yellow, and the major hydrogen-bonding interactions with MelB$_{St}$ are indicated in broken line. All sugar-binding residues are labeled in pink color and the transmembrane helices are shown in parentheses brackets. A loose cation-binding pocket was proposed for this D59C mutant, and all possible residues for Na^+ binding are labeled in black.

ficity determinant pocket hosts the specific galactosyl moiety.[3]

This sugar specificity determinant pocket is formed by both of the N- and C-terminal helical bundles involving in five helices (I, IV, V, X, and XI), particularly the helices I and IV (Figure 1(b)). Two negatively charged Asp residues at positions 19 (helix I) and 124 (helix IV), and two positively charged residues Lys18 (helix I) and Arg149 (helix IV), as well as Trp128 (helix IV), form multiple hydrogen-bonding interactions with all four hydroxyl groups on the galactosyl moiety. All Cys mutants at position 18, 19, 124, or 128 completely abolished all three-mode melibiose active transport coupled to H^+, Li^+, or Na^+.[10]

The D59C MelB$_{St}$ with the mutation at its cation-binding site has been determined as an uniport mutant (Figure 1). This single-site Cys mutation selectively abolishes the cation binding and all three modes of melibiose active transport, but still catalyzes melibiose transport and support melibiose fermentation,[3] as well as the melibiose exchange.[10] Interestingly, D59C MelB$_{St}$ exhibits superior protein stability and sugar-binding affinity.[3] Both Asp55 and Asp59 (helix II) have been shown to contribute to Na^+ binding.[13–18] In the structure [pdb id,7L17], the position 59 has much less solvent exposure, and Asp55 is involved in a salt-bridge with Lys377 (helix XI). Single-Cys mutants on Asn58 (helix II) or Thr121(helix IV) have been shown to selectively inhibit Na^+-coupled melibiose transport with less or no inhibition on the transport coupled to Li^+;[10] in addition, the MelB ortholog of *Klebsiella pneumoniae* (MelB$_{Kp}$) uses H^+ or Li^+ (but not Na^+) as the coupling cation,[19–21] where Ala residue is present on position Asn58. In the structure, Thr121 is in close proximity to both Asp55 and Asp59, and the Asn58 side chain is extended toward to the membrane. Since the D59C mutant, which was used for the structure determination, does not bind a cation, the cation binding was not resolved and the detailed coordination is unknown in MelB$_{St}$ (Figure 1(c)); interestingly, the cation site directly connects to the bound galactosyl moiety. The helix IV seems to host both cation- and sugar substrate-binding sites, which can dictate the coupling between the two substrates and contribute to the observed cooperative binding.[18,22–24]

In this study, we performed molecular dynamics simulations to characterize the Na^+ and Li^+ binding to MelB$_{St}$ and focused on the less-characterized Thr121 (helix IV). As shown previously, a single-site T121C mutant selectively inhibited melibiose transport coupled to Na^+ or H^+ cations without obvious inhibition of the Li^+-coupled transport.[10] Bio-informatics studies show that this Thr residue is evolutionally strictly conserved even across those functionally unrelated, likely cation-coupled transporters,[3] including the MFSD2A. The potential importance of Thr121 in the cation-binding site was also indicated by a lethal mutation on the identical position T159M in MFSD2A.[25] While three structures of Na^+-coupled

MFS transporters have been determined, none solved the cation binding problem. Here we presented evidence that Thr121 is part of the cation-binding site of $MelB_{St}$ and is essential for Na^+ binding, but not for H^+ or Li^+ binding. In addition, this study also provided important information supporting the argument that the charge balance of this cation-binding pocket plays an important role in $MelB_{St}$ protein stability.

Results

Binding of Na^+ or Li^+ with $MelB_{St}$ by molecular dynamics simulations

To simulate the Na^+ and Li^+ binding, the WT $MelB_{St}$ derived from the D59C structure [PDB, 7L17] was subjected to all-atom MD simulations embedded in a lipid bilayer consisting of 1-palmitoyl-2-oleoyl-sn-glycero-3-phosphoethanolamine (POPE) and 1-palmitoyl-2-oleoyl-sn-glycero-3-phosphoglycerol (POPG) with a ratio similar to that in the *E. coli* membranes.[26] After nearly 1 μs of MD simulations of $MelB_{St}$ in complex with melibiose and either Na^+ or Li^+, the overall protein structure remains stable. The Na^+ is stably coordinated by 5 coordinating oxygen atoms from 4 residues (Asp55, Asn58, Asp59, and Thr121) with an average coordination bond length of 2.3 Å (Figure 2(a)). The Asp55 and Asp59 are stabilized by salt-bridges with Lys377 (helix XI), and Thr121 is stabilized through a hydrogen bond with Gly117. The Li^+ is stably coordinated by 4 coordinating oxygen atoms mainly from only 3 residues (Asp55, Asn58 and Asp59) with an average coordination bond length of 2.0 Å (Figure 2(a and b)). In contrast to Na^+, the coordination of Li^+ by the Thr121 is less stable.

The Li^+ binding to $MelB_{St}$ is different from Na^+. Li^+ is closer to the Asp55, Asn58 and Asp59 on helix II. The probability distribution of the closest distance between the hydroxyl oxygen on the side chain of Thr121 (OG1(T121)) and the Li^+ or Na^+ ions revealed that there is a single peak for Na^+-OG1 distances, but there are two peaks for Li^+-OG1 distance (Figure 2(c)). The first peaks are located at 2.1 Å and 2.4 Å for the Li^+ and Na^+, respectively, which correspond to direct coordination between the OG1 atom of Thr121 and the cation. The Na^+-OG1 distance at the first peak is slightly larger than the Li^+-OG1 distance due to the larger radius of the Na^+. Importantly, in the distance distribution of Li^+-OG1, there is a second peak at ~4.1 Å, which arises from the breakage of the coordination interaction between the Li^+ and the OG1 atom of Thr121. In other words, during the 1 μs simulation, there is significant amount of time when the Thr121 did not coordinate the Li^+. In contrast, the second peak is absent in the distance distribution of Na^+-OG1, which indicates stable coordination of the Na^+ by the Thr121 throughout the 1 μs simulation.

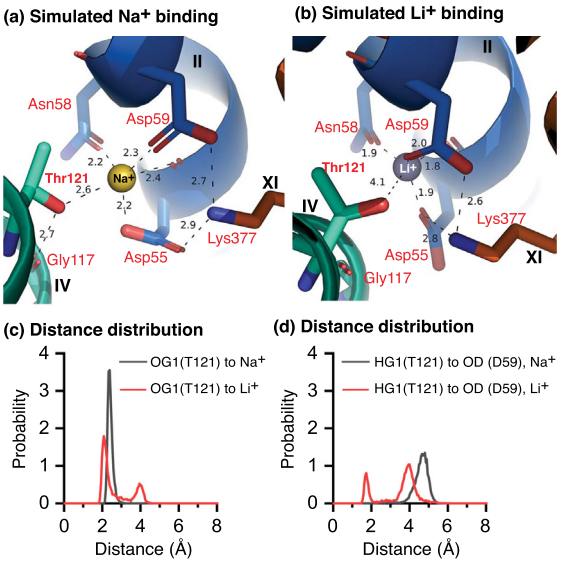

Figure 2. Cation-binding sites for Na^+ or Li^+ simulated by MD simulations. All-atom MD simulations of the WT were performed in lipid bilayer as described in the Methods. Na^+ (a) and Li^+ (b) were manually placed in the binding site. **(a & b)** The structures of the binding site of Na^+ and Li^+ taken from the two 1 μs MD trajectories. The Na^+ and Li^+ are represented by the yellow and purple balls, respectively, and the side chains of neighboring atoms are represented by sticks. The backbone of the protein is represented as ribbons. The coordination interactions between the cation and the neighboring residues are indicated by dashed lines with the separation distances labeled. **(c)** Distribution of the closest distance between the hydroxyl oxygen atom on the side chain of the Thr121 (OG1(T121)) and the Na^+ or Li^+ ions. **(d)** Distribution of closest distance between the hydroxyl hydrogen atom on the side chain of the Thr121 (HG1(T121)) and the carboxyl oxygen atoms of the Asp59 (OD(D59)). The distributions for the Li^+ and Na^+ bound $MelB_{St}$ are colored in red and blue, respectively. The Thr121 stably binds the Na^+ but not the Li^+ during the 1 μs MD simulations. During the 1 μs simulations of Li^+-bound $MelB_{St}$, the Thr121 side chain flipped between the bound Li^+ and Asp59.

A closer inspection into the dynamics of the Li^+-bound $MelB_{St}$ revealed that the hydroxyl group on the side chain of Thr121 frequently donates hydrogen bond to the carboxyl group of the Asp59. To quantify the observation, the distribution of the closest distance between the hydrogen atom on the hydroxyl group of the Thr121 (HG1(T121)) and the carboxyl oxygen atoms (OD(D59)) was analyzed. For the Li^+-bound $MelB_{St}$, there are two peaks for the distances between HG1 of Thr121 and OD of Asp59. The first peak appears at ~1.7 Å, corresponding to the hydrogen bond distance between the HG1 and the OD atoms. This peak is missing in the Na^+-bound $MelB_{St}$ (Figure 2(d)). It is likely that Li^+ is favorably attracted by Asp55, Asp59 and

Asn58 so that the Thr121 is released to form hydrogen bond with Asp59.

Site-directed mutagenesis of $MelB_{St}$ Thr121

To further characterize the role of Thr121, a total number of 11 single-site mutants on Thr121 were constructed using the WT $MelB_{St}$ as the template. Non-polar residues (Ala, Gly, Pro, or Leu including Met, the lethal mutation at the homolog site of human MFSD2A) and polar residues (Ser, Asn, or Cys) were generated to test if the hydroxyl group on the Thr sidechain and its precise positioning are important. Asp and Arg mutants were included to test how a negative charge or bulky positive charge affect the cation binding. The bulkiest Trp residue was for testing the volume effect.

Protein expression

The membrane expression levels of the $MelB_{St}$ WT and mutants in the *E. coli* DW2 cells was examined by western blotting. As judged by an anti-His tag antibody, all Thr121 mutants exhibited similar levels of membrane expression, with Cys, Gly, and Ala mutants slightly better than others; however, as shown in the histogram, all mutations inhibited the protein expressions by about 50% when compared to the WT (Figure 3; Table 1).

[^{3}H]Melibiose transport with intact cells

The *E. coli* DW2 (*melA*$^+$*melB*$^-$*lacZ*$^-$*Y*$^-$) intact cells expressing the WT or individual single-site mutants were used for [^{3}H]melibiose transport assay at 0.4 mM (specific activity of 10 mCi/mmol) in the absence or presence of 20 mM NaCl or LiCl. While the chromosomal *melA*$^+$ encoding α-galactosidase is present, it is not expressed without the induction melibiose.[27,28] Thus, this trace-flux assay determines melibiose accumulation against concentration gradient.[29] As showed previously,[2] the WT catalyzed melibiose accumulation couples to H^+ in the absence of Na^+ and Li^+ (Figure 4); in the presence of Na^+ or Li^+, the initial rates and steady-state level of melibiose accumulation are largely increased. The Na^+-coupled transport is slightly greater than the Li^+-coupled melibiose transport (Figure 4). The effects of Thr121 mutations on all three modes of transport are varied (Table 1), and most mutations exhibited stronger inhibitions on melibiose active transport couped to Na^+ or H^+ than the coupling with Li^+.

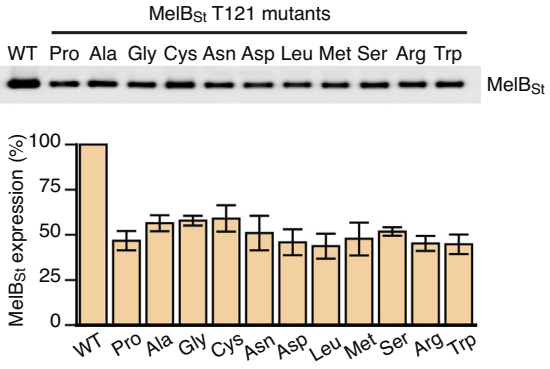

Figure 3. Membrane expression and western blotting. Membranes containing the WT and mutant $MelB_{St}$ in a buffer containing 50 mM NaPi, pH 7.5, 100 mM NaCl, 20 mM melibiose and 10% glycerol were prepared as described in Methods. An aliquot of 20 μg membrane proteins of each sample were analyzed by SDS-15% PAGE, and $MelB_{St}$ proteins were detected by western blotting using anti-His tag antibody as described in Methods.

Several mutants (Pro, Ser, Cys, Ala, Gly, Asn, Asp, or Leu mutations) altered the cation selective preference (Figure 4); thus, their symport activities with Li^+ were better than that with Na^+. Remarkably, the Cys, Ser, Pro and Ala mutants remained excellent melibiose transport coupled to Li^+. With regard to the H^+-coupled transport, only the T121P mutant retained the high steady-state level of melibiose accumulation. With regard to the Na^+-coupled transport, most mutations showed severe inhibitions, and T121C and T121S mutants retained the best activity, but still less than 50% of the WT. T121P, A, G mutants completely lost the Na^+ coupling. With the Asn, Asp and Leu mutants, all the three modes of transport activities were largely inhibited.

The Met mutation largely inhibited all three modes of transport, but retained the Na^+-coupled transport better than Li^+- or H^+-coupled activities. Arg and Trp mutants with a bulky sidechain (the T121R mutant also with a positive charge) then completely abolished all three modes of transport (Figure 4), while both proteins were expressed at a level comparable to all other mutants (Figure 3(a)).

Melibiose fermentation

Melibiose fermentation activity was assessed by growing the cells on the MacConkey agar plates containing 30 mM melibiose as the sole carbohydrate source and sufficient Na^+. WT $MelB_{St}$ fermented melibiose well and the colonies and agar background turned to magenta color (Figure 4, inset; Table 1), an indicator for a fast melibiose transport and degrees of acidification.[30] The negative control DW2 cells with no MelB grew as yellow colonies, a sign for no melibiose fermentation, which could be yielded from no or very slow melibiose transport, or no α-galactosidase. Among all mutants, the T121R and T121W exhibited yellow colonies, indicating no fermentation, which is consistent with the results from the active transport. Most other mutants (including Cys, Asn, Asp, Leu and Met mutants) fermented melibiose similar to

Table 1 Summary.

		WT	Ser	Cys	Ala	Pro	Gly	Asn	Asp	Leu	Met	Arg	Trp
Expression (%)[a]		100	51.83 ± 2.3*	59.05 ± 7.3	56.41 ± 4.4	46.73 ± 5.4	57.89 ± 2.7	50.97 ± 9.6	45.89 ± 7.1	43.74 ± 7.0	47.76 ± 9.1	45.26 ± 4.2	44.69 ± 5.4
Fermentation[b]		Good	Poor	Good	S	S	S	Good	Good	Good	Good	No	No
Transport at 30 min (%)[c]	H^+	100	47.8 ± 10.69	16.5 ± 2.01	34.0 ± 3.41	106.8 ± 4.54	18.5 ± 2.28	8.7 ± 2.83	8.0 ± 2.66	4.4 ± 1.42	49.6 ± 11.56	−1.0 ± 0.78	0.4 ± 0.12
	Na^+	100	22.8 ± 0.18	23.0 ± 1.21	3.7 ± 0.25	11.3 ± 0.13	9.1 ± 1.10	2.5 ± 0.28	2.7 ± 0.12	1.0 ± 0.11	30.5 ± 4.02	0.5 ± 0.27	0.2 ± 0.12
	Li^+	100	84.7 ± 1.18	75.3 ± 0.55	93.6 ± 5.48	109.2 ± 2.39	41.7 ± 4.15	22.5 ± 0.76	21.9 ± 0.83	15.0 ± 1.86	31.0 ± 5.09	−0.5 ± 0.39	0 ± 0.05
Sugar binding (IC_{50}, mM)[d]	H^+	+	+	+	+	+	+	+	+	+	+	+	−
	Na^+	+	+	+	+	+	+	+	+	+	+	+	−
	Li^+	0.73 ± 0.04	1.99 ± 0.12	2.58 ± 0.03	2.48 ± 0.04	5.77 ± 0.52	+	+	+	+	+	+	−
Na^+ binding ($K_{0.5(Na+)}$, mM)[e]		0.83 ± 0.25	8.24 ± 0.22	30.34 ± 1.81	/**	/	+	+	−	−	+	−	−
Li^+ binding ($K_{0.5(Na+)}$, mM)[f]		1.88 ± 0.35	3.48 ± 0.43	0.67 ± 0.01	0.58 ± 0.05	0.42 ± 0.09	+	+	+	+	+	−	−
Soluble $MelB_{St}$ at 52 °C (%)[g]	Na^+	41.6 ± 3.5	10.85 ± 4.0	3.89 ± 0.2	3.99 ± 0.5	3.32 ± 1.6	2.14 ± 2.1	3.50 ± 1.2	7.94 ± 1.7	1.38 ± 0.3	1.84 ± 1.2	2.87 ± 1.6	2.35 ± 0.1
	Li^+	44.89 ± 4.0	33.78 ± 1.3	46.62 ± 1.3	51.51 ± 4.2	7.99 ± 2.2	8.68 ± 1.5	21.25 ± 3.0	3.79 ± 1.2	19.62 ± 0.5	31.51 ± 3.2	2.55 ± 0.9	2.73 ± 1.5
T_m (°C)[h]	Li^+	62.54 ± 0.32		60.30 ± 0.18	64.71 ± 0.23								
	Li^+ + Mel	63.87 ± 0.04		61.03 ± 0.13									
pKa estimation[i]	Mel	8.75 ± 0.02***	7.75 ± 0.02	8.36 ± 0.03	8.75 ± 0.02	9.18 ± 0.02							

[a] Relative expression derived from Figure 3.

[b] Interpretation of fermentation results presented in Figure 4; S, Colonies were small but red.

[c] Relative transport activity at 30-min time point presented in Figure 4.

[d] All data were from Trp → D^2G assays. IC_{50} were carried out with $MelB_{St}$ in nanodiscs and the presence of Li^+ (Figure 7). The bound D^2G was displaced by melibiose binding as described in the Methods. For most cases, the FRET binding results in Figure 5 were explained as positive (+) or negative (−) qualitatively.

[e] $K_{0.5(Na+)}$, Na^+ stimulation constant on the Trp → D^2G FRET carried out with $MelB_{St}$ in nanodiscs as determined in Figure 6. For Ala and Pro mutants, no fitting due to lack of feature of the titration curve. For other cases, the Na^+ binding data in Figure 5 were explained as positive (+) or negative (−) qualitatively.

[f] $K_{0.5(Li+)}$, Li^+ stimulation constant on the Trp → D^2G FRET were carried out with $MelB_{St}$ in nanodiscs as determined in Figure 6. For Ala and Pro mutants, no fitting due to lack of feature of the titration curve. For other cases, the Li^+ binding data in Figure 5 were explained as positive (+) or negative (−) qualitatively.

[g] Data were from Figure 8, and the relative amount of soluble $MelB_{St}$ proteins compared to the total $MelB_{St}$ after 52 °C treatment as described in Methods.

[h] The melting temperature was determined by CD spectroscopy in Figure 9. All purified protein samples contain 0.01% DDM and 100 mM LiCl in the assay buffer.

[i] The calculated p*K*a values by PROPKA program as described in Methods.

*, SE, number of tests = 2–3.

**, No fitting.

***, SE, number of tests = 1000.

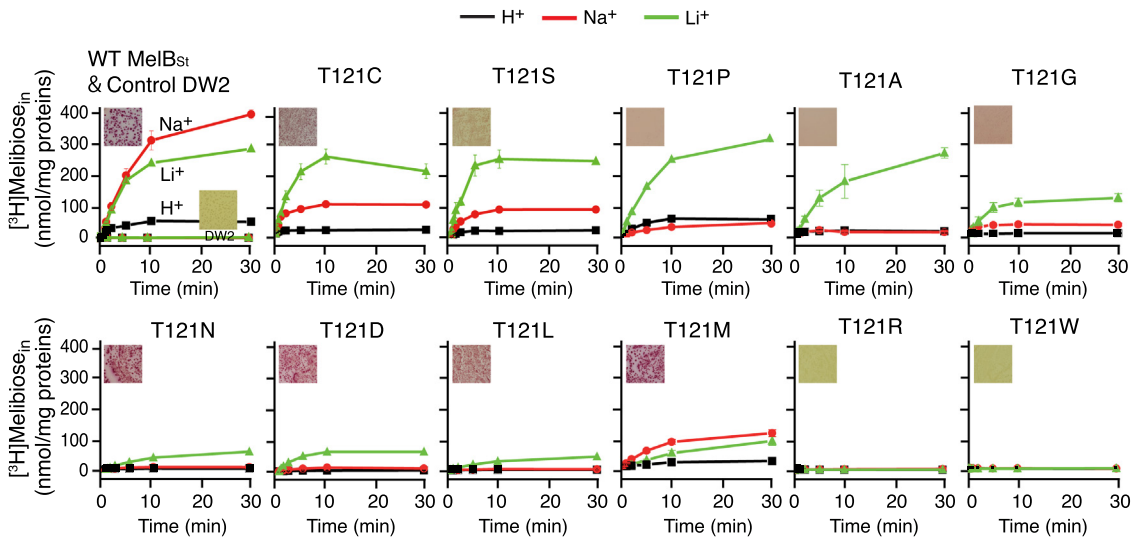

Figure 4. Melibiose transport time course and fermentation. $MelB_{St}$ expression in *E. coli* DW2 (*melA*$^+$*melB*$^-$-*lacY*$^-$) cells and active transport assay were described in Methods. The transport was carried out at 0.4 mM [^{3}H] melibiose in the absence or presence of 20 mM NaCl or 20 mM LiCl at 23 °C. Accumulated melibiose was plotted against incubation time. *E. coli* DW2 cells that do not carry the expressing plasmid were included as the negative control and presented in the same panel for the positive control, the WT $MelB_{St}$. The results of melibiose fermentation on MacConkey agar plate containing 30 mM melibiose as the sole carbohydrate source were presented in each transport panel. Red colonies, normal melibiose fermentation; yellow colonies, no fermentation; pink colonies, reduced fermentation rates.

the WT, although the Asn, Asp, and Leu mutants showed no Na^+- or H^+-coupled activities. The T121S formed pink colonies, indicating a low-level melibiose fermentation.

The Pro, Ala, and Gly mutants, interestingly, had a growth problem and formed colonies at small sizes on the selective media; however, they grew normally on the regular LB agar plates or LB broth media. While the size is small, the colonies are red indicating fermentation of melibiose.

Measurement of substrate binding by Trp → D^2G FRET with RSO membrane vesicles

Trp → D^2G FRET is a well-established assay for the detection of substate binding to MelB including galactosides, Na^+, or Li^+ binding.[2,31,32] It is based on the overlapping spectra of MelB Trp emission and dansyl excitation. The FRET signal can be displaced by MelB substrates but not by sucrose or other non-MelB substrate sugars, which show the specific interaction of fluorescent analogue dansyl-2-galactoside (D^2G) to MelB. The specific binding can be detected in native membrane samples,[2,30,33] purified in detergent,[10,18,22] or reconstituted into proteoliposomes.[26] To assess the mutational effects *in situ*, right-side-out (RSO) membrane vesicles were prepared by osmotic lysis from *E. coli* DW2 cells carrying the WT or individual mutants to determine the binding of substrates (galactoside, Na^+ or Li^+). With the WT $MelB_{St}$ (Figure 5), D^2G at a final concentration of 10 μM (similar to the K_d value) was added into the RSO vesicle sample, and fluorescent intensity was recorded at an exciting wavelength at 290 nm and an emission wavelength at 490 nm that is maximal in the Trp → dansyl galactoside FRET spectra in $MelB_{St}$.[2] Consecutive addition of melibiose decreased the fluorescent intensity; on a separate trace, addition of water only exhibited a small dilution effect. The difference in the fluorescent intensity between the two traces reflects the Trp → bound dansyl galactoside FRET, i.e., the evidence for the binding of galactosides.

Addition of NaCl or LiCl prior to the melibiose displacement increased the fluorescent intensity. This increase is mainly derived by an increase in the number of D^2G binding as a result of positive binding cooperativity between galactoside and cation.[18,34] In addition, Trp environmental changes induced by the cation binding could be another factor. With the WT $MelB_{St}$, the total intensity increase induced by Na^+ is significantly smaller than that by Li^+, which may indicate the two ternary complexes might adopt two different conformations.[2]

The T121 mutants exhibited varied phenotypes on the Trp → D^2G FRET measurement (Figure 5; Table 1). Except for the T121W mutant, all other mutants displayed galactosides binding. Further, T121N, T121S, and T121R mutants in the absence of Na^+ or Li^+ exhibited the D^2G-binding signal similar to that of the WT; however, none of

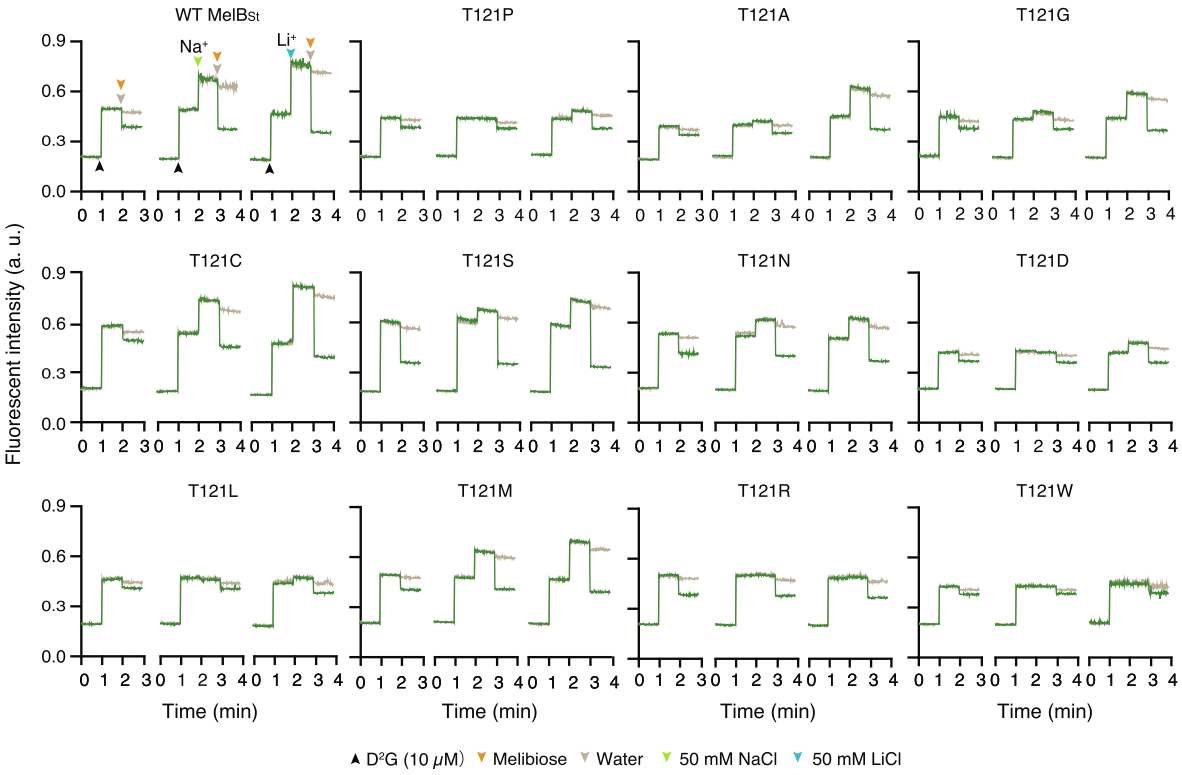

Figure 5. Substrate binding determined by Trp → D^2G FRET assay. Right-side-out (RSO) membrane vesicles in a Na^+-free buffer prepared from *E. coli* DW2 cells expressing $MelB_{St}$ at 1 mg/ml were mixed with D^2G at 10 μM (black arrows) and fluorescence intensity at 490 nm were recorded using an excitation wavelength 290 nm. At an interval of 1 min, melibiose at a final concentration of 130 mM (pink arrows), NaCl at 50 mM (green arrow), or LiCl at 50 mM (blue arrow), was supplemented as indicated. Each panel contains two traces, one with water (gray arrow) instead of melibiose but at equal volume for the correction of dilution effect.

them catalyzed H^+-coupled melibiose transport as the WT did.

Pro mutant retained the binding for D^2G, melibiose, and Li^+, with reduced FRET intensity changes, but lost the Na^+ binding. In consistent to the transport data, the T121P mutant selectively eliminated Na^+ binding and Na^+-coupled melibiose symport but retained the other two modes, i.e., H^+/melibiose and Li^+/melibiose symport.

Ala and Gly mutants also exhibit galactoside binding and Li^+ stimulation, but the Na^+-binding signal was largely reduced. T121C, T121N, T121M, and T121S mutants showed good binding signals for both Na^+ or Li^+; T121D and T121L lost Na^+ binding.

Determination of cation binding by measuring the cation-stimulation constants ($K_{0.5}$) with lipid nanodiscs

The increase in FRET intensity ($_{diff}$FRET) induced by Na^+ or Li^+ only reflects the binding qualitatively. The FRET intensity changes derived from some mutants are too small to determine quantitatively the cation-binding affinity. The attempts to generate purified proteins with the routine $MelB_{St}$ purification protocol failed due to poor stability of these mutants in detergents. Thus, to maintain the stability as shown in Figure 8, reconstitution into lipid nanodiscs immediately following the elution step during the affinity purification was applied.

With the Trp → D^2G FRET assay (Figure 6(a)), instead of adding 50 mM NaCl or LiCl, stepwise titrations of Na^+ or Li^+ were carried out till no further FRET change occurred. The cation simulation constant ($K_{0.5}$), which reflects the cation-binding affinity, can be determined from a hyperbolic function. With the lipids nanodiscs containing the WT $MelB_{St}$, the $K_{0.5(Na+)}$ and $K_{0.5(Li+)}$ values were 0.83 mM and 1.88 mM, respectively, which are in a range of the results from RSO membrane vesicles (Table 1).[2,27,30] The conserved T121S mutant exhibited 10-fold reduced Na^+-binding affinity with $K_{0.5(Na+)}$ of 8.24 ± 0.22 mM, whereas the affinity to Li^+ was only decreased by

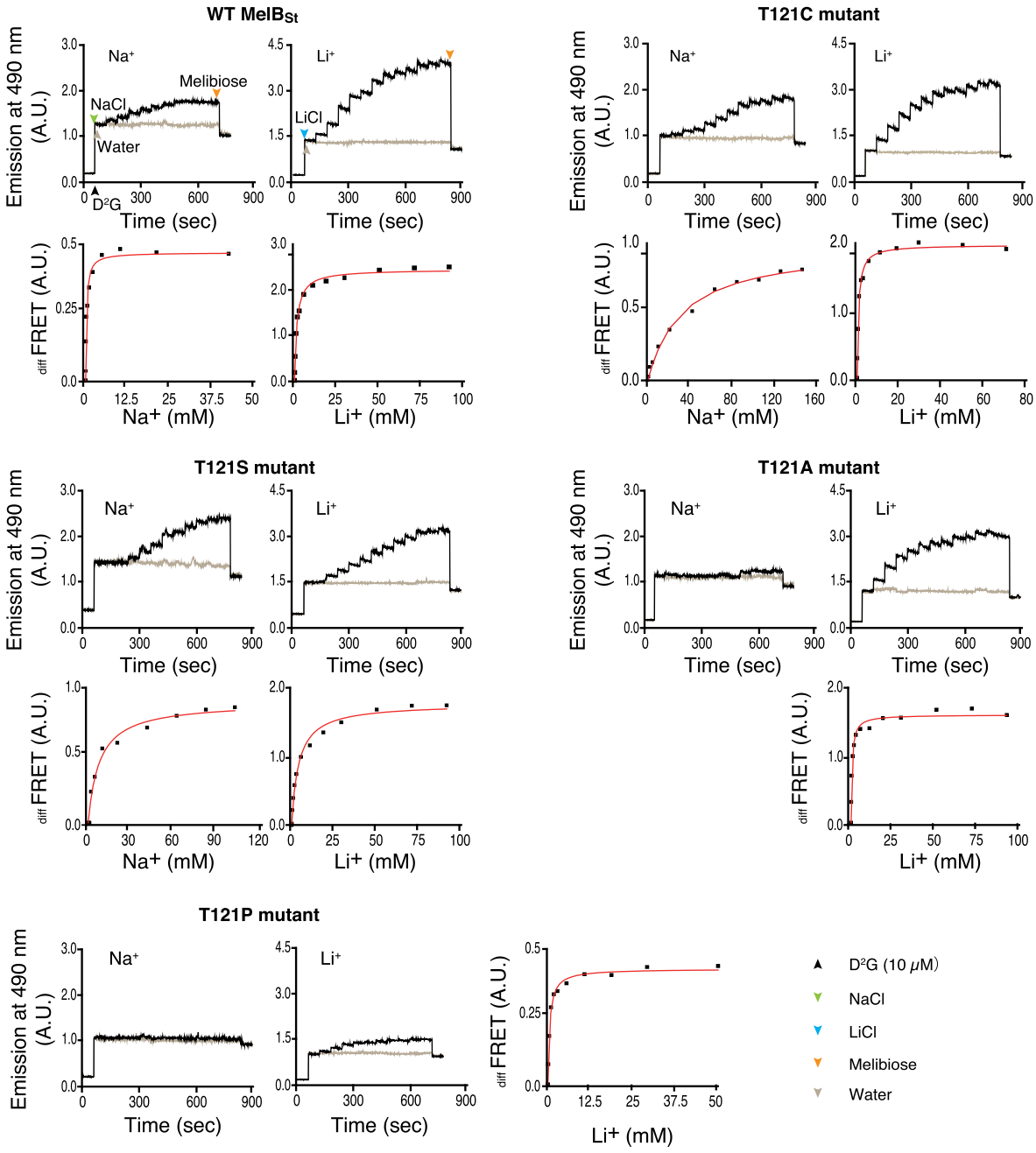

Figure 6. Cation-binding affinity. Trp → D^2G FRET assay was used to determine cation-binding affinity by measuring the stimulation constant on the FRET. $MelB_{St}$ proteins were reconstituted into lipid nanodiscs as described in the Methods, and the Trp → D^2G FRET was recorded at 490 nm as described in the legend of Figure 5. NaCl or LiCl, at a 1 min interval, was added stepwise until no change in FRET signal was approached. Addition of an identical volume of water at each step was used for the control. The $K_{0.5}$ determination was carried out as described in the Methods.

less than 2-fold. T121C mutation largely inhibited the Na^+ binding with a $K_{0.5(Na+)}$ value of 30.34 ± 1. 81 mM, which is greater than 30-fold poor than that for the WT, but its affinity to Li^+ is 3-fold increased with a $K_{0.5(Li+)}$ of 0.67 ± 0.01 mM.

With T121P and T121A mutants, there was no Na^+ binding detected even with increased NaCl concentration to greater than 500 mM. Both mutants, however, exhibited an increased binding affinity to Li^+ by 3 ∼ –4 -fold and the $K_{0.5(Li+)}$

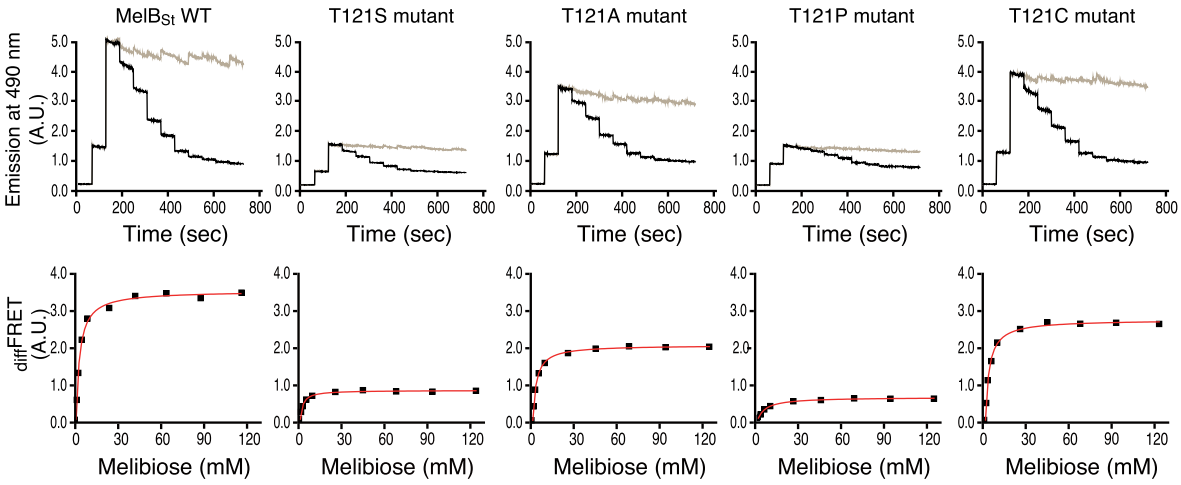

Figure 7. Melibiose binding affinity. Trp → D^2G FRET assay was used to determine the melibiose-binding affinity expressed as IC_{50} for melibiose displacement of D^2G binding. Stepwise displacements of D^2G by melibiose at increasing concentrations were measured on a time trace and IC_{50} values were determined as described in the Methods.

values for T121P and T121A mutants were 0.42 ± 0.09 mM and 0.58 ± 0.05 mM, respectively.

Determination melibiose-binding affinity by determining the melibiose concentration to displace half-maximal Trp → D^2G FRET (IC_{50}) with lipid nanodiscs.

With the Trp → D^2G FRET assay, instead of adding the saturating concentration of melibiose, titrations of melibiose step by step were carried out till no further FRET change occurred (Figure 7). The melibiose IC_{50}, which reflects the melibiose affinity, can be determined from a hyperbolic function. With the lipids nanodiscs containing the WT $MelB_{St}$, the IC_{50} for melibiose to displace 50% bound D^2G values were 2.73 ± 0. 04 mM in the presence of Li^+ (Table 1). As indicated from the time-trace records, melibiose binding affinities to the mutants including T121S, T121C and T121A are in the similar range of the WT, and T121P mutant exhibited slightly greater IC_{50} (5.77 ± 0.52 mM).

Thermostability detected by western blotting

To test the thermostability of the mutant proteins (Figure 8(a)), membranes (10 mg/mL) in a Na^+- and melibiose-containing buffer (50 mM NaPi, pH 7.5, 200 mM NaCl, and 20 mM melibiose) were solubilized with a detergent dodecyl-β-D-maltopyranoside (DDM) (1.5%) on ice, then incubated at 52 °C or 54 °C for 90 min. After an ultracentrifugation to remove aggregates, equal volume of supernatant was analyzed by SDS-15% PAGE and western blotting, using untreated membranes diluted with water instead of DDM as the control. The WT $MelB_{St}$ can be detected even after 90-min heat incubation at 54 °C; however, for all mutants, hardly any $MelB_{St}$ is visualized even after 52 °C treatment.

To test the Li^+ effect (Figure 8(b)), all membranes were extensively washed by the same buffer but containing LiCl at 200 mM instead of NaCl. Interestingly, the presence of Li^+ largely increased the protein stability for several mutants (Figure 8, Histogram); such as the thermostability of T121A and T121C mutants are similar to the WT. With a treatment at 54 °C, the $MelB_{St}$ protein band can be detected clearly with T121S mutant and visible for T121D and T121M mutants. Further, between the two salts, the stability of the WT $MelB_{St}$ is greater in the presence of Li^+ than Na^+.

Melting temperature (T_m) detected by CD spectroscopy

For a quantitative analysis, the WT $MelB_{St}$ and T121A and T121C mutants were purified in DDM in the presence of NaCl and subjected to CD spectra analysis and thermal denaturation testes for determining the melting temperature (T_m) (Figure 9), as described previously.[22,26] In this study, we focused on the mutational effect. Overall, the CD spectra in the absence or presence of sub-strates were undistinguishable (Figure 9(a)), fea-tured with strong negative ellipticity sub-maxima at 209 nm and 222 nm. The thermal denaturation tests were performed at temperatures between 25 and 90 °C and the ellipticity changes at 210 nm were recorded to monitor the unfolded fractions (Figure 9 (b)). The T_m value, at which 50% protein unfolded, for the WT bound with $Li^±$ is 62.63 ± 0.53 °C, and ternary state with both $Li^±$ and melibiose is 63.89 ±

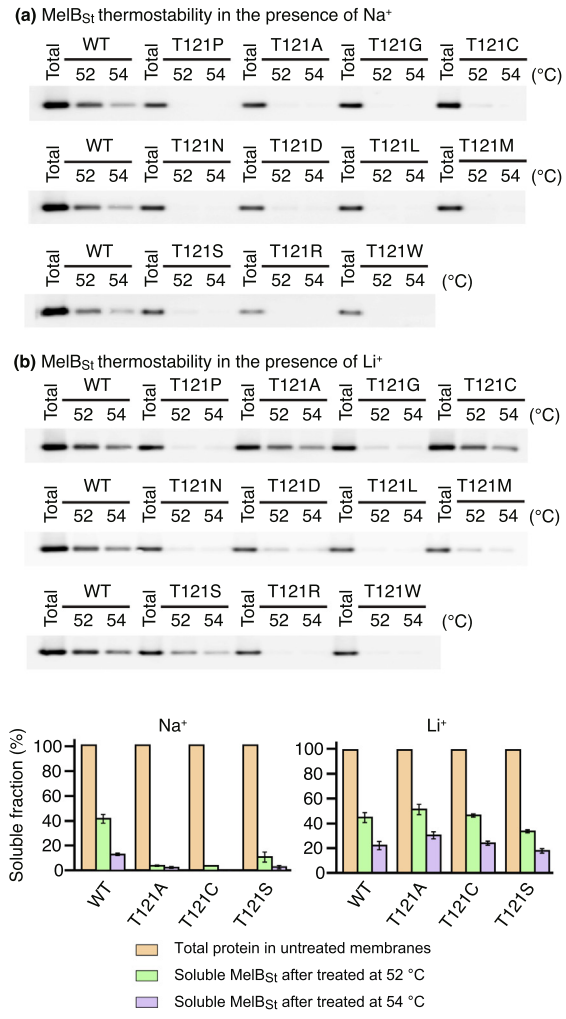

Figure 8. Thermostability tests detected by western blotting. (a) Thermostability in the presence of Na^+. The membrane samples at a protein concentration of 10 mg/ml were mixed with detergent 1.5% DDM for 90 min on ice, and the samples were then incubated in increased temperatures of 52 °C and 54 °C, respectively, for another 90 min before ultracentrifugation at 355,590 *g* for 45 min. Equal volume of the supernatants was analyzed by SDS-15%PAGE using the membranes containing same amount of membrane proteins for the DDM extract as the control for total $MelB_{St}$. **(b)** Thermostability in the presence of Li^+. To remove Na^+, membrane samples were extensively washed with LiCl-containing buffer (50 mM Tris–HCl, pH 7.5, 100 mM LiCl, 20 mM melibiose and 10% glycerol) and subjected to the test as described in panel *a*. Histograms, the soluble fractions were derived from panel *a* (in the presence of Na^+) and panel *b* (in the presence of Li^+). Pink bar, the total membrane proteins; green or blue bars, soluble $MelB_{St}$ after treated at 52 °C or 54 °C, respectively. The number of tests is 2, and each variation bar indicated the SE values.

0.04 °C (Table 1). Mutant T121C exhibited slighted reduced T_m values, and mutant T121A showed slightly increased T_m values of 65.36 ± 0.88 °C. The T_m results are consistent with the data from the thermostability tests detected by western blotting (Figure 8).

Estimated pKa of Asp59 in the WT $MelB_{St}$ and mutants

Previous competitive assay of Na^+ binding as a function of pH with isotherm titration calorimetry (ITC) revealed the p*K*a value of $MelB_{St}$ cation-binding site is about 6.25 or 6.59 in the absence or presence of melibiose.[18] Currently, the Asp59 is suggested to be the sole sidechain responsible for the proton binding in $MelB_{St}$. To further examine if the local hydrophobicity near the Thr121 affects the p*K*a of Asp59, four Thr121 mutants (including Ser, Cys, Pro and Ala mutations) were created computationally, and the p*K*a values of Asp59 in the WT and each mutant were estimated by molecular dynamics simulations combined with the PROPKA program (Table 1).[35,36] It is well-known that it is challenging to computationally predict the *absolute* p*K*a values of ionizable residues deeply buried in proteins, and our simple PROPKA calculations indeed predicts higher p*K*a values than the experimental measurements. However, the *relative* changes in the calculated p*K*a between the WT and mutants under the same simulation conditions are often more reliable and could provide useful information. Both the T121S and T121C mutants decrease the Asp59 p*K*a relative to the WT due to the presence of more hydrophilic residues (Table 1). In contrast, the calculated p*K*a values for the T121A and T121P mutants are either unaffected or elevated, respectively, due to the presence of side chains with similar or more hydrophobicity compared to that in the WT.

Discussion

A transporter that uses Na^+ as the coupling cation can often use Li^+ and/or H^+. For most Na^+-coupled bacterial secondary transporters, their cation site has not been extensively studied. In $MelB_{St}$ and $MelB_{Ec}$, the specificity, selectivity and stoichiometry have been well characterized.[1,2,18,37–39] All studies support that the three cations H^+, Na^+, and Li^+ share the same binding pocket.[2,18,40–42] In $MelB_{St}$, previous ITC measurements determined the absolute K_D values for Na^+ and H^+, which are 0.64 mM and 0.56 μM (pK_a of 6.25), respectively.[18] The binding affinities increase in the presence of melibiose with a cooperativity number of 8 and 2, respectively; thus, $K_{D(Na+)}$ and $K_{D(H+)}$ are decreased to 90 μM and 0.26 μM, respectively.[18] Melibiose affinity was also increased in the presence of Na^+, so a positive cooperativity of melibiose and Na^+ binding has been firmly established, which has been proposed to be the core principle of symport mechanisms.[22]

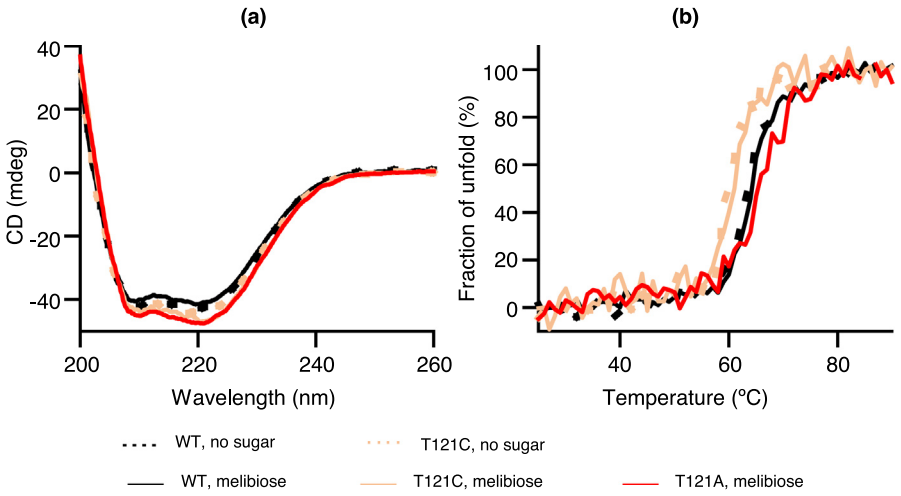

Figure 9. Determination of melting temperature by thermo-denaturation monitored by CD spectroscopy. (a) CD spectra. $MelB_{St}$ at a protein concentration of 4 μM in the CD assay buffer (20 mM NaPi, pH 7.5, 100 mM LiCl, 10% glycerol, and 0.01% DDM) in the absence or presence of melibiose at 50 mM were prepared for the measurements. The CD spectra were recorded between 200 and 260 nm at 25 °C after subtracted from each corresponding buffer control. **(b)** Thermal denaturation. The CD ellipticity changes were recorded at 210 nm at a 1 °C interval with temperature ramping at 1 °C per minute, and expressed as a percentage of unfolded fraction. Black, WT $MelB_{St}$; pink, T121C mutant; red, T121A mutant. Dashed line, no sugar; solid line, with 50 mM melibiose.

While $MelB_{St}$ cation binding was extensively characterized biochemically, our knowledge at molecular levels is still limited. The high-resolution 3D structures for three Na^+-coupled MFS transporters were solved[3,11,12]; unfortunately, none of them resolved the Na^+ binding. Our all-atom MD simulations in this study show that Asp55, Asn58, Asp59, and Thr121 of $MelB_{St}$ contributes to the cation binding (Figure 2), which is consistent with previous functional analysis and extend the knowledge of cation binding in $MelB_{St}$. The Na^+ is stably coordinated by five coordinating atoms from all four residues with an average coordination bond length of 2.3 Å. This Na^+ coordination pattern in $MelB_{St}$ is similar to that observed in the MFSD2A[12] or the multidrug and toxic compound extrusion (MATE) transporters.[43] The Li^+ is stably coordinated by four coordinating atoms from three residues with an average coordination bond length of 2.0 Å, and the coordination by the Thr121 is less stable. Interestingly, the helix II contributes three critical residues for cation coordination (Asp55, Asn58, and Asp59), and the helix IV hosting the major sugar-binding residues (Asp124, Trp128, Tyr120) also contributes the Thr121 residue for cation coordination. The Na^+ and Li^+ are only slightly different in their ionic radii, and the difference in the two simulated binding modes are small, but the two cations affect MelB's conformational change and transport activity very differently. For example, melibiose change rate in the presence of Na^+ is fast, but Li^+ inhibits the melibiose exchange rate.[2] The novel insights into the difference of Na^+ and Li^+ binding interactions with $MelB_{St}$ presented here may provide important clues for exploring the mechanistic effects on the activities and coupling mechanisms of MelB in the future.

The Thr121 residue forms stable coordination interaction with the Na^+ but not the Li^+. Our systematic mutagenesis in combination of melibiose transport, substrate binding, and stability assays consistently support the observation from the MD simulations that Thr121 residue is part of the cation binding pocket and essential for the binding to Na^+, but not necessary for the binding of Li^+. Any Thr121 mutants that can bind Na^+ are also capable in binding of Li^+. All Thr121 mutants that can significantly retain the Na^+ binding and Na^+-coupled active transport contain a polar group (either O or S) on the γ (Ser or Cys) or the δ (Met) position. Interestingly, T121N mutation also carries a carbonyl O at δ position, but the amide group may interrupt the binding of Na^+ and Li^+. The T121C mutant retains the highest transport activity coupled to Na^+; it has an unaltered initial transport rate, but the steady-state accumulation level was only 30% of the WT (Figure 4; Table 1).

The γ carbon in the methyl group on the Thr121 sidechain is in close proximity to Asp59 (Figure 1 (c)), and it might partially contribute to the local hydrophobicity around Asp59 and an elevated p*K*a of this residue for the binding of H^+. Neither Cys nor Ser contains this hydrophobic methyl group, and accordingly the H^+-coupled active transport of melibiose by the two mutants are also poor. With regard to the steady-state level of the H^+-coupled melibiose accumulation, the T121P mutant is the best, followed by Met, Ala, and Ser mutants, albeit with a large difference in activity levels. All other

mutants nearly completely lost the H^+/melibiose symport activity. The computationally estimated p*K*a values of Asp59 in the T121S, T121C, T121A and T121P mutants are consistent with our interpretations that the local hydrophobic environment modulates the proton affinity of Asp59, thereby affecting the H^+-coupled melibiose transport (Table 1).

Placing Pro or Ala at position Thr121 increased the affinity for Li^+, with little effects on the Li^+/melibiose symport activity (Table 1; Figure 4). In contrast, these residues with no or a hydrophobic carbon sidechain selectively eliminated Na^+ binding (Figures 5 and 6), which narrowed the cation specificity of $MelB_{St}$. Placing the small polar residues Cys or Ser on Thr121 largely inhibited the Na^+ binding and the Na^+-coupled melibiose symport, but caused only mild inhibitions of Li^+ binding, with an unnoticeable change in the Li^+-coupled transport. These mutations largely altered cation selectivity. When introducing a residue with a large, bulky, or hydrophobic sidechain, the binding to either Na^+ or Li^+ were severely inhibited. The different effects on Na^+ or Li^+ binding from Cys and Ser compared with Pro and Ala may suggest that the precise positioning of a polar group is required for coordinating Na^+. All of our experimental data support that the binding of Li^+ only involves a subset of the Na^+-binding site, which is consistent with the MD simulations results showing that Li^+ coordination number in $MelB_{St}$ is less than that of Na^+. Overall, the results indicate that Thr121 is essential for Na^+ binding, but it is not necessary for the Li^+ binding or the H^+ binding.

Protein stability is critical for structural and functional characterizations experimentally. The stability of $MelB_{St}$ is strongly influenced by the charge balance of the cation-binding pocket. This binding site contains two negatively charged residues (Asp55 and Asp59), two polar residues (Asn58 and Thr121), and a positively charged Lys377 residue. Ly377 is positioned between the Asp55 and Asp59, which yields an unbalanced charge distribution (2 negative and 1 positive). In the D59C mutant crystal structure, Lys377 forms a salt-bridge interaction with Asp55.[3] This single D59C mutation of $MelB_{St}$, by removing one negative charge and neutralizing charge distribution in the cation-binding site, largely increased thermostability of $MelB_{St}$ by ~6 °C.[3] Further, the D55C mutation also increased thermostability by 2 °C.[22] The WT $MelB_{St}$ with an empty cation-binding site is less stable, and the binding of the cation Na^+ increases the thermostability by 1.5 °C and the binding of Na^+ in the presence of melibiose increases the thermostability by 2.6 °C.[22]

In this study, the protein stability of Thr121 mutants exhibited a clear cation dependence. Due to a weak or lack of Na^+ binding, all mutants showed largely reduced stabilities in the presence of Na^+ (Figure 6). Remarkably, neutralization of the cation-binding site for mutants T121A, T121C and T121S by a bound Li^+ regained the protein thermostability. Especially in the presence of Li^+, the T121A mutant exhibited higher Li^+ binding affinity (Table 1) and also slightly greater T_m than that of the WT (Table 1; Figures 8 and 9). Taken all together, a charge-unbalanced cation-binding site causes protein less stable or unstable, and $MelB_{St}$ can be stabilized by the binding of Na^+ or Li^+, or a mutatation to remove one negative charge. This finding supports the view that the charge balance of the cation-binding pocket modulates $MelB_{St}$ stability. The results provide useful knowledge and important insights for generating stable protein samples for structural and functional studies.

Materials and Methods

Materials and regents

[1-^{3}H]Melibiose (5.32 Ci/mmol) was custom synthesized by *PerkinElmer* and unlabeled melibiose was purchased from *Acros Organics* (*Fisher Scientific*). MacConkey agar media (lactose free) was purchased from Difco. Detergent n-dodecyl-β-D-maltopyranoside (DDM) were purchased from Anatrace. 2′-(*N*-dansyl) aminoalkyl-1-thio-β-D-galactopyranoside (D^2G) was kindly provided by Drs. Gerard Leblanc and the late H. Ronald Kaback. *E. coli* Extract Polar was purchased from Avanti. All other materials were reagent grade and obtained from commercial sources. Oligodeoxynucleotides were synthesized by Integrated DNA Technologies. All mutants were constructed by QuickChange™ Site-Directed Mutagenesis Kit (Invitrogen), and confirmed by DNA sequencing analysis.

Bacterial strains and plasmids

E. coli DW2 strain (*melA*$^+$, *ΔmelB*, *ΔlacZY*) was used for expression and functional analyses. The expression plasmid pK95 ΔAH/$MelB_{St}$/$CHis_{10}$ encoding the $MelB_{St}$ with a His_{10}-tag at the C terminus[2,38] was used as the template for constructing the site-directed mutagenesis.

Cell growth for transport assay and protein expression

E. coli DW2 cells transformed with the plasmid carrying MelB were grown in Luria-Bertani (LB) broth with 100 mg/L ampicillin in a 37 °C shaker overnight. The overnight cell growth was diluted by 5% to fresh LB broth with 0.5% glycerol and 100 mg/L of ampicillin. Constitutive overpression was obtained by shaking at 30 °C for 5 h for the functional tests and for examining the protein expression level.

[1-^{3}H]Melibiose transport assay

E. coli DW2 cells expressing $MelB_{St}$ were washed with 50 ml of 100 mM KP_i (pH 7.5) three times, followed by washing with the assay buffer (50 ml 100 mM KP_i, pH 7.5, 10 mM $MgSO_4$). The cell pellets were resuspended with the assay buffer and adjusted to A_{420} = 10 (~0.7 mg proteins/ml). The transport was initiated by mixing 50 μL of cells with 2 μL of 10 mM [^{3}H]melibiose at a specific activity of 10 mCi/mmol in the absence or presence of 500 mM NaCl or 500 mM LiCl, respectively, which yielded a final concentration of 0.4 mM melibiose in the absence or presence of 20 mM Na^+ or 20 mM Li^+, respectively. The transport time courses were carried out by separating the cells from solutions at zero, 5 s, 10 s, 30 s, 1 m, 2 m, 5 m, 10 m, and 30 m by a dilution and fast filtration. The filters were subjected to the radioactivity measurement using a Liquid Scintillation Counter. The radioactivity was converted to nmol melibiose/mg proteins. The *E. coli* DW2 cells without a plasmid were used as the negative control.

Melibiose fermentation on MacConkey agar plates

E. coli DW2 cells were transformed with a plasmid carrying the WT or mutants and plated on MacConkey agar plates containing 30 mM melibiose, 100 mg/L of ampicillin, and incubated at 37 °C. After 18 h, the plates were viewed and photographed immediately. Formation of magenta color colonies after 18 h is indicative of a normal melibiose fermentation; pink colony, reduced fermentation; yellow colony indicates on melibiose fermentation due to poor transport rates,

Membrane expression and western blotting

Cells were grown as described for the transport assay. After 7 h shaking at 30 °C, cells were washed with 50 mM NaP_i, pH 7.5, resuspended with the same buffer, and broken by sonication. The unbroken cells or debris were removed by centrifugation, and the supernatant were subjected to ultracentrifugation at 62,000 rpm for 30 min in a Beckman rotor Ti 70. The membrane pellets were resuspended with 50 mM NaP_i, pH 7.5, 200 mM NaCl, 10% glycerol, and 20 mM melibiose. After protein assay, 20 μg of total membranes was loaded on to SDS-15% PAGE. The gel was transferred onto the PVDF membrane by the Trans-Blot Turbo transfer system (Bio-Rad) at 1.3 A, 25 V for 20 min. The PVDF membrane was blocked by 3% BSA in TBST buffer (25 mM Tris–HCl, pH 7.5, 150 mM NaCl, and 0.05% tween-20) overnight, and then washed with TBST buffer for 15 min twice. The washed membrane was used to react with the HisProbe™-HRP conjugate (Thermo Scientific) in TBST with 1.0% BSA for 1 h, and then washed three times with TBST for 15 min. $MelB_{St}$ protein was detected using the SuperSignal West Pico chemiluminescent substrate (*Thermo Scientific*) by the ImageQuant LAS 4000 Biomolecular Imager (GE Health Care Life Science).

Protein thermostability assay in the presence of Na^+ or Li^+

Membranes in buffer containing Na^+ and melibiose (50 mM NaP_i, pH 7.5, 200 mM NaCl, 10% glycerol, and 20 mM melibiose) at a final protein concentration of 10 mg/ml were mixed with 1.5% DDM for 90 min on ice. The membrane extracts were then incubated at two increased temperatures of 52 °C and 54 °C, respectively, for another 90 min before ultracentrifugation at 355,590*g* in a Beckman OptimaTM MAX ultracentrifuge using a TLA-100 rotor for 45 min at 4 °C. Equal volume of the supernatants were analyzed by SDS-15%PAGE and western blotting. The membranes containing same amount of total protein that were used for the DDM extract was loaded as the control for total $MelB_{St}$.

For test Li^+ effects, the membranes in the Na^+-containing buffer were diluted by 50-fold with Li^+-containing buffer (50 mM Tris–HCl, pH 7.5, 200 mM LiCl, 10% glycerol, and 20 mM melibiose) with other components unchanged, and ultracentrifuged at 62,000 rpm using Ti 70 rotor for 30 min. The pellets were washed with the same buffer by a 50-fold dilution with sonication. The pellets after ultracentrifugation were resuspended in the same Li^+-containing and subjected to the thermostability testes as described above.

Protein concentration assay

The Micro BCA Protein Assay (Pierce Biotechnology, Inc.) was used to determine the protein concentration assay.

Right-side-out (RSO) membrane vesicles preparation

The $MelB_{St}$ was expressed in the *E. coli* DW2 as described above, and RSO membrane vesicles were prepared by osmotic lysis and resuspended in 100 mM KPi as described.[2,44,45]

Affinity purification of the WT and mutant $MelB_{St}$

Cell growth for a large-scale production of the WT $MelB_{St}$ and single-site Thr121 mutants from *E. coli* DW2 cells *(melA$^+$melB, lacZY)* as described.[10,46] Briefly, the cells were grown in Luria–Bertani broth supplemented with 50 mM KPi, pH 7.0, 45 mM $(NH_4)SO_4$, 0.5% glycerol, and 100 mg/liter ampicillin[46] The initial protocols for membrane preparation and $MelB_{St}$ purification by cobalt-affinity chromatography after extraction by 2% DDM were

adapted as described previously.[3] $MelB_{St}$ protein was eluted with 250 mM imidazole in a buffer containing 50 mM NaPi, pH 7.5, 100 mM NaCl, 0.01% DDM, and 10% glycerol, and dyalyzed to change the buffer conditions.

Overexpression and purification of membrane scaffold protein (MSP)

Overexpression of the membrane scaffold protein MSP1D1E3 with N-terminal 7-His tag followed by spacer sequence and tobacco etch virus (TEV) protease cleavage site (mass 32.6 kDa) from a plasmid pMSP1E3D1 (Addgene; #20066) was carried out in the *E. coli* BL21 (DE3) strain. MSP1D1E3 yields nanodiscs with a diameter of ~12.1 nm.[47] The cells were grown in LB media containing 0.5% glucose and 30 mg/L kanamycin at 37 °C; protein expression was induced by adding 1 mM IPTG at an A_{600} of ~0.6 for 2–3 h. The MSP from the cell lysates were purified with metal-affinity purification using INDIGO Ni-Agarose (*Cube Biotech*). The eluted MSP at 300 mM imidazole were dialyzed at 4 °C against 20 mM Tris–HCl, pH 7.5, and 100 mM NaCl and concentrated to ~8 mg/ml. To remove the His tag, a 5 mL of 21.5 mg MSP1D1E3 protein was mixed with 0.5 mL of His-tagged TEV protease (1.67 mg/ml in 25 mM KPi, 200 mM NaCl, 10% glycerol, 2 mM EDTA, 10 mM DTT, pH 8.0), at a ratio of 1:20 (TEV/ MSP1D1E3, mol/mol), and incubated for 48 h at 4 °C. Processed MSP was separated from His-tagged TEV protease and unprocessed His-tagged MSP by Ni-agarose chromatography as a flowthrough, concentrated to ~6–8 mg/ml, frozen in liquid nitrogen, and stored at −80 °C.

Reconstitution of $MelB_{St}$ into phospholipid bilayer nanodiscs

A stepwise reconstitution was adapted from the reported protocols.[22,48] Briefly, in a 2-ml reaction, 2 mg of the purified $MelB_{St}$ in DDM at a concentration of 1 mg/ml was mixed with 12.6 mg of *E. coli* polar lipids extract from a stock of 40 mg lipids/ml (50 mM) in 7.5% DDM, yielding a protein:lipid ratio of 1:420 (mol/mol) or 1:6.3 (mg/mg). The protein/lipid mixture was incubated for 10 min on ice; MSP1D1E3 protein was added at a 6:1 molar ratio of MSP1D1E3:$MelB_{St}$, followed by incubation at 23 °C with mild stirring for 30 min. The detergents were removed using 1 g Bio-Beads SM-2 (500 mg beads per 1 mg $MelB_{St}$) with mild stirring at 4 °C for 2 h, followed by overnight incubation after adding another portion of Bio-Beads SM-2 (300 mg). Bio-Beads SM-2 was removed by centrifugation at 20,000 g for a few minutes at 4 °C, and the reconstituted phospholipid bilayer nanodiscs were collected from the supernatant.

Reconstituted nanodiscs were further isolated by metal-affinity purification using Ni-NTA beads. The elute containing $MelB_{St}$ in nanodiscs was further dialyzed against a ligand-free buffer without a detergent (20 mM Tris–HCl, pH 7.5, 50 mM Choline Chloride (ChoCl), and 10% glycerol. Protein concentration was measured at A_{280} nm with an extinction coefficient (ε = 135,110) based on 1 $MelB_{St}$ and 2 MSP1D1E3 molecules. $MelB_{St}$ lipid nanodiscs were aliquoted, flash-frozen in liquid nitrogen, and stored at −80 °C.

Trp → dansyl fluorescence resonance energy transfer (FRET)

Steady-state fluorescence measurements were performed with an AMINCO-Bowman series 2 spectrometer with RSO membrane vesicles containing $MelB_{St}$ at 1 mg/ml in 100 mM KP_i, pH 7.5. Using an excitation wavelength at 290 nm, the emission intensity was recorded at 490 nm. On a time-trace, D^2G, NaCl or LiCl, then melibiose were sequentially added into the RSO vesicles solution at a 1 min-interval. An identical volume of water instead of melibiose was used for the control on a separate trace.

Determination of the cation stimulation constant of Na^+ ($K_{0.5(Na+)}$) and $Li^±$ ($K_{0.5(Li+)}$) on the Trp → dansyl FRET intensity

The reconstituted lipid nanodisc samples at a $MelB_{St}$ concentration of ~1 μM were used to increase the binding signal. On the same experimental setup as described above, titration of Na^+ or Li^+ after adding 10 μM D^2G were performed. An identical volume of water was used for the control. The increase in the intensity after each cation addition was corrected by the dilution effect and plotted as a function of the accumulated cation centration. The $K_{0.5}$ value was determined by fitting a hyperbolic function to the data (OriginPro).

Determination of IC_{50} for melibiose displacement of the Trp → dansyl FRET intensity

Trp → dansyl FRET was used to determine melibiose affinity using the reconstituted lipids nanodiscs. After the addition of 10 μM D^2G and LiCl, melibiose was added consecutively till no further decrease in the FRET intensity was reached. Addition of the identical volume of water was used for the correction of dilution effect. The decrease in FRET was plotted as a function of melibiose concentration. IC_{50} was determined by the hyperbolic fitting to data.

CD spectroscopy and melting temperature (T_m) determination

The CD measurements were carried out using Jasco J-815 spectrometer equipped with a Peltier MPTC-490S temperature-controlled cell holder unit. $MelB_{St}$ at 4 μM in 20 mM NaPi, 100 mM LiCl,

10% glycerol, and 0.01% DDM at a pH 7.5 in the absence or presence of 50 mM melibiose. An aliquot of 180-μL $MelB_{St}$ sample was placed in 1-mm quartz cuvette on the temperature-controlled cell holder. CD spectra for a wavelength range of 200–260 nm were collected at data pitch of 0.1 nm using a band width of 1 nm and scanning speed of 100 nm/min by using Jasco Spectra Measurement software (V.2). Each spectrum was corrected by subtraction with corresponding buffer in the absence of $MelB_{St}$.

The T_m determination was carried out by thermal denaturation tests at temperatures between 25 and 90 °C. Ellipticity at 210 nm was recorded at a 1 °C interval with the temperature ramp rate at 1 °C per minute, and plotted against temperature. The T_m values were defined as the temperature leading to 50% unfolding, which was determined by fitting the data to the Jasco Thermal Denaturation Multi Analysis Module.

All-atom molecular dynamics simulation

The crystal structure of the D59C mutant of the $MelB_{St}$ (pdb, 7L17) was used as the starting structure for the simulation of the WT $MelB_{St}$. The Cys at position 59 was mutated back to Asp59. The protein was embedded in a lipid bilayer consisting of POPE and POPG. The ratio of POPE vs. POPG was 7:2, similar to the membrane composition of *E. coli*, and the total number of lipid molecules was 288. The lipid bilayer was capped by water molecules on each side, and either LiCl or NaCl ions were inserted among the water molecules to generate a solution of ~0.16 M concentration. The melibiose was inserted into the sugar binding site based on the crystal structure of the α-NPG. The simulation system contained ~131,000 atoms, and the periodic boundary condition was ~99 Å × 99 Å × 131 Å. The CHARMMGUI web interface[49] was employed to setup the system.

The following simulation procedures were applied to each of the two system setups, i.e. the $MelB_{St}$ + LiCl + melibiose and the $MelB_{St}$ + NaCl + melibiose. The system was first optimized with the heavy atoms of protein and lipids harmonically restrained (using 1000 kJ/mol/Å^2 force constant), followed by 130 ps of dynamics at 300 K temperature in the constant NVT ensemble. The restraints were then gradually reduced to zero over 10 ns of dynamics in the constant NPT ensemble at 300 K temperature and 1 atm. Finally, 30 ns of dynamics in the constant NPT ensemble with the same temperature and pressure was carried out for equilibration with no restraints. After equilibration, 1 μs of dynamics in the constant NPT ensemble with the same temperature and pressure was carried out to generate the production trajectory. The temperature was maintained by a Langevin thermostat with a friction coefficient of 1 ps^{-1}. The trajectory was propagated with a 2 fs timestep, and the lengths of all bonds that involve a hydrogen atom are constrained. Throughout all simulations, the CHARMM36 force field was used to simulate the protein, lipid, melibiose and ions.[50–53] The particle mesh Ewald method[54] with a tolerance of 5×10^{-4} was used to calculate the electrostatic interactions. The cutoff for van der Waals interactions was chosen as 12 Å. The water molecules were treated by the TIP3P model.[55] The classical MD equilibration was performed using the OPENMM software package.[56]

Estimation of pKa values of $MelB_{St}$ Asp59

The WT and four computationally created mutants (T121S, T121C, T121A and T121P) were subjected to p*K*a calculation using the PROPKA program.[35,36] For each system, 100 ns MD simulation was performed in the constant NPT ensemble (T = 300 K, P = 1 atm) with Asp59 in the protonated state and other ionizable residues in their standard protonated states (deprotonated Asp, Glu, His and protonated Thr, Ser, Cys, Lys, Arg, Tyr). In the aqueous solution capping the lipid bilayer, 0.16 M KCl was added. Other simulation parameters remained the same as mentioned above. During the MD simulation, none of the K^+ ions penetrated into the cation-binding site. One thousand snapshots were extracted from each of the five MD trajectories with a 100 ps interval, and each snapshot was subjected to the pKa calculation of Asp59 using the PROPKA program.[35,36] The statistical uncertainty of the average p*K*a value for each system was obtained by bootstrapping over 1000 random samples of all snapshots.

CRediT authorship contribution statement

Satoshi Katsube: Investigation, Visualization. **Ruibin Liang:** Conceptualization, Resources, Investigation, Formal analysis, Writing – original draft, Writing – review & editing, Visualization. **Anowarul Amin:** Investigation. **Parameswaran Hariharan:** Methodology, Formal analysis. **Lan Guan:** Investigation, Visualization, Formal analysis, Writing – original draft, Writing – review & editing, Visualization.

DATA AVAILABILITY

Data will be made available on request.

Acknowledgements

The authors thank Dr. Gerard Leblanc for the *E. coli* DW2 cells and MelB expression plasmid. S.K. currently is a recipient of Grant-in-Aid for JSPS Overseas Research Fellowship. R.L. is

supported by startup funds and Texas Tech University High-Performance Computing Center. This work was supported by the National Institutes of Health grants R01GM122759 and R21NS105863 to L.G.

Conflict of interest

The authors declare that they have no conflicts of interest with the contents of this article.

Received 22 February 2022;
Accepted 14 April 2022;
Available online 22 April 2022

Keywords:
cation-coupled symporter;
membrane protein stability;
3-D structure;
ligand binding;
structure and function analysis;
MD simulations

† Current address: National Cancer Institute, 9609 Medical Center Dr, Rockville, MD 20850, United States.

Abbreviations:
WT, wild type; $MelB_{St}$, *Salmonella typhimurium* melibiose permease; $MelB_{Kp}$, *Klebsiella pneumoniae* melibiose permease; $MelB_{Ec}$, *Escherichia coli* melibiose permease; *E. coli*, *Escherichia coli*; MSFD2A, Na^+-dependent phospholipids transporter; DDM, dodecyl-β-D-maltopyranoside; DDMB, dodecyl melibioside; α-NPG, α-nitrophenyl galactoside; D^2G, dansyl-2-galactoside; RSO, right-side-out; FRET, fluorescence resonance energy transfer; $K_{0.5(Na+)}$, the stimulation constant of Na^+ for the Trp→dansyl FRET intensity; $K_{0.5(Li+)}$, the stimulation constant of Li^+ for the Trp→dansyl FRET intensity; CD, circular dichroism; T_m, melting temperature; MD simulations, molecular dynamics simulations; p*K*a, acid dissociation constants

References

1. Niiya, S., Moriyama, Y., Futai, M., Tsuchiya, T., (1980). Cation coupling to melibiose transport in *Salmonella typhimurium*. *J. Bacteriol.* **144**, 192–199.
2. Guan, L., Nurva, S., Ankeshwarapu, S.P., (2011). Mechanism of melibiose/cation symport of the melibiose permease of *Salmonella typhimurium*. *J. Biol. Chem.* **286**, 6367–6374.
3. Guan, L., Hariharan, P., (2021). X-ray crystallography reveals molecular recognition mechanism for sugar binding in a melibiose transporter MelB. *Commun Biol* **4**, 931.
4. Guan, L. (2021) Glucose/Sugar Transport in Bacteria. In: *Encyclopedia of Biological Chemistry* ((eds.), I. J. J. ed., 3rd Ed., Elsevier, Oxford.
5. Yan, N., (2015). Structural Biology of the Major Facilitator Superfamily Transporters. *Annu. Rev. Biophys.* **44**, 257–283.
6. Drew, D., North, R.A., Nagarathinam, K., Tanabe, M., (2021). Structures and General Transport Mechanisms by the Major Facilitator Superfamily (MFS). *Chem. Rev.* **121**, 5289–5335.
7. Nguyen, L.N., Ma, D., Shui, G., Wong, P., Cazenave-Gassiot, A., Zhang, X., Wenk, M.R., Goh, E.L., et al., (2014). Mfsd2a is a transporter for the essential omega-3 fatty acid docosahexaenoic acid. *Nature* **509**, 503–506.
8. Anzai, T., Matsumura, Y., (2019). Topological analysis of TMEM180, a newly identified membrane protein that is highly expressed in colorectal cancer cells. *Biochem. Biophys. Res. Commun.* **520**, 566–572.
9. Yasunaga, M., Saijou, S., Hanaoka, S., Anzai, T., Tsumura, R., Matsumura, Y., (2019). Significant antitumor effect of an antibody against TMEM180, a new colorectal cancer-specific molecule. *Cancer Sci.* **110**, 761–770.
10. Ethayathulla, A.S., Yousef, M.S., Amin, A., Leblanc, G., Kaback, H.R., Guan, L., (2014). Structure-based mechanism for Na(+)/melibiose symport by MelB. *Nature Commun.* **5**, 3009.
11. Cater, R.J., Chua, G.L., Erramilli, S.K., Keener, J.E., Choy, B.C., Tokarz, P., Chin, C.F., Quek, D.Q.Y., et al., (2021). Structural basis of omega-3 fatty acid transport across the blood-brain barrier. *Nature* **595**, 315–319.
12. Wood, C.A.P., Zhang, J., Aydin, D., Xu, Y., Andreone, B.J., Langen, U.H., Dror, R.O., Gu, C., et al., (2021). Structure and mechanism of blood-brain-barrier lipid transporter MFSD2A. *Nature* **596**, 444–448.
13. Pourcher, T., Zani, M.L., Leblanc, G., (1993). Mutagenesis of acidic residues in putative membrane-spanning segments of the melibiose permease of *Escherichia coli*. I. Effect on Na(+)-dependent transport and binding properties. *J. Biol. Chem.* **268**, 3209–3215.
14. Zani, M.L., Pourcher, T., Leblanc, G., (1993). Mutagenesis of acidic residues in putative membrane-spanning segments of the melibiose permease of *Escherichia coli*. II. Effect on cationic selectivity and coupling properties. *J. Biol. Chem.* **268**, 3216–3221.
15. Ding, P.Z., Wilson, T.H., (2001). The effect of modifications of the charged residues in the transmembrane helices on the transport activity of the melibiose carrier of *Escherichia coli*. *Biochem. Biophys. Res. Commun.* **285**, 348–354.
16. Granell, M., Leon, X., Leblanc, G., Padros, E., Lorenz-Fonfria, V.A., (2010). Structural insights into the activation mechanism of melibiose permease by sodium binding. *PNAS* **107**, 22078–22083.
17. Fuerst, O., Lin, Y., Granell, M., Leblanc, G., Padros, E., Lorenz-Fonfria, V.A., Cladera, J., (2015). The melibiose transporter of *Escherichia coli*: Critical contribution of lys-377 to the structural organization of the interacting substrate binding sites. *J. Biol. Chem.* **290**, 16261–16271.
18. Hariharan, P., Guan, L., (2017). Thermodynamic cooperativity of cosubstrate binding and cation selectivity of *Salmonella typhimurium* MelB. *J. Gen. Physiol.* **149**, 1029–1039.
19. Hama, H., Wilson, T.H., (1992). Primary structure and characteristics of the melibiose carrier of *Klebsiella pneumoniae*. *J. Biol. Chem.* **267**, 18371–18376.
20. Hama, H., Wilson, T.H., (1993). Cation-coupling in chimeric melibiose carriers derived from Escherichia coli and Klebsiella pneumoniae. The amino-terminal portion is crucial for Na+ recognition in melibiose transport. *J. Biol. Chem.* **268**, 10060–10065.

21. Hama, H., Wilson, T.H., (1994). Replacement of alanine 58 by asparagine enables the melibiose carrier of Klebsiella pneumoniae to couple sugar transport to Na+. *J. Biol. Chem.* **269**, 1063–1067.
22. Hariharan, P., Guan, L., (2021). Cooperative binding ensures the obligatory melibiose/Na+ cotransport in MelB. *J. Gen. Physiol.* **153**
23. Bassilana, M., Damiano-Forano, E., Leblanc, G., (1985). Effect of membrane potential on the kinetic parameters of the Na(+) or H(+) melibiose symport in *Escherichia coli* membrane vesicles. *Biochem. Biophys. Res. Commun.* **129**, 626–631.
24. Cordat, E., Leblanc, G., Mus-Veteau, I., (2000). Evidence for a role of helix IV in connecting cation- and sugar-binding sites of *Escherichia coli* melibiose permease. *Biochemistry* **39**, 4493–4499.
25. Guemez-Gamboa, A., Nguyen, L.N., Yang, H., Zaki, M.S., Kara, M., Ben-Omran, T., Akizu, N., Rosti, R.O., et al., (2015). Inactivating mutations in MFSD2A, required for omega-3 fatty acid transport in brain, cause a lethal microcephaly syndrome. *Nature Genet.* **47**, 809–813.
26. Hariharan, P., Tikhonova, E., Medeiros-Silva, J., Jeucken, A., Bogdanov, M.V., Dowhan, W., Brouwers, J.F., Weingarth, M., et al., (2018). Structural and functional characterization of protein-lipid interactions of the Salmonella typhimurium melibiose transporter MelB. *BMC Biol.* **16**, 85.
27. Guan, L., Jakkula, S.V., Hodkoff, A.A., Su, Y., (2012). Role of Gly117 in the cation/melibiose symport of MelB of *Salmonella typhimurium*. *Biochemistry* **51**, 2950–2957.
28. Tikhonova, E.B., Ethayathulla, A.S., Su, Y., Hariharan, P., Xie, S., Guan, L., (2015). A transcription blocker isolated from a designed repeat protein combinatorial library by in vivo functional screen. *Sci. Rep.* **5**, 8070.
29. Markham, K.J., Tikhonova, E.B., Scarpa, A.C., Hariharan, P., Katsube, S., Guan, L., (2021). Complete cysteine-scanning mutagenesis of the Salmonella typhimurium melibiose permease. *J. Biol. Chem.* **297**, 101090.
30. Jakkula, S.V., Guan, L., (2012). Reduced Na(+) affinity increases turnover of *Salmonella enterica* serovar Typhimurium MelB. *J. Bacteriol.* **194**, 5538–5544.
31. Maehrel, C., Cordat, E., Mus-Veteau, I., Leblanc, G., (1998). Structural studies of the melibiose permease of *Escherichia coli* by fluorescence resonance energy transfer. I. Evidence for ion-induced conformational change. *J. Biol. Chem.* **273**, 33192–33197.
32. Cordat, E., Mus-Veteau, I., Leblanc, G., (1998). Structural studies of the melibiose permease of *Escherichia coli* by fluorescence resonance energy transfer. II. Identification of the tryptophan residues acting as energy donors. *J. Biol. Chem.* **273**, 33198–33202.
33. Amin, A., Hariharan, P., Chae, P.S., Guan, L., (2015). Effect of Detergents on Galactoside Binding by Melibiose Permeases. *Biochemistry* **54**, 5849–5855.
34. Hariharan, P., Guan, L., (2014). Insights into the inhibitory mechanisms of the regulatory protein IIA(Glc) on melibiose permease activity. *J. Biol. Chem.* **289**, 33012–33019.
35. Sondergaard, C.R., Olsson, M.H., Rostkowski, M., Jensen, J.H., (2011). Improved Treatment of Ligands and Coupling Effects in Empirical Calculation and Rationalization of pKa Values. *J. Chem. Theory Comput.* **7**, 2284–2295.
36. Olsson, M.H., Sondergaard, C.R., Rostkowski, M., Jensen, J.H., (2011). PROPKA3: Consistent Treatment of Internal and Surface Residues in Empirical pKa Predictions. *J. Chem. Theory Comput.* **7**, 525–537.
37. Bassilana, M., Pourcher, T., Leblanc, G., (1987). Facilitated diffusion properties of melibiose permease in *Escherichia coli* membrane vesicles. Release of co-substrates is rate limiting for permease cycling. *J. Biol. Chem.* **262**, 16865–16870.
38. Pourcher, T., Leclercq, S., Brandolin, G., Leblanc, G., (1995). Melibiose permease of *Escherichia coli*: large scale purification and evidence that H(+), Na(+), and Li(+) sugar symport is catalyzed by a single polypeptide. *Biochemistry* **34**, 4412–4420.
39. Wilson, T.H., Ding, P.Z., (2001). Sodium-substrate cotransport in bacteria. *BBA* **1505**, 121–130.
40. Lopilato, J., Tsuchiya, T., Wilson, T.H., (1978). Role of Na (+) and Li(+) in thiomethylgalactoside transport by the melibiose transport system of *Escherichia coli*. *J. Bacteriol.* **134**, 147–156.
41. Damiano-Forano, E., Bassilana, M., Leblanc, G., (1986). Sugar binding properties of the melibiose permease in *Escherichia coli* membrane vesicles. Effects of Na(+) and H (+) concentrations. *J. Biol. Chem.* **261**, 6893–6899.
42. Mus-Veteau, I., Leblanc, G., (1996). Melibiose permease of *Escherichia coli*: structural organization of cosubstrate binding sites as deduced from tryptophan fluorescence analyses. *Biochemistry* **35**, 12053–12060.
43. Castellano, S., Claxton, D.P., Ficici, E., Kusakizako, T., Stix, R., Zhou, W., Nureki, O., McHaourab, H.S., et al., (2021). Conserved binding site in the N-lobe of prokaryotic MATE transporters suggests a role for Na(+) in ion-coupled drug efflux. *J. Biol. Chem.* **296**, 100262.
44. Kaback, H.R., (1971). Bacterial Membranes. *Methods Enzymol.* **XXII**, 99–120.
45. Short, S.A., Kaback, H.R., Kaczorowski, G., Fisher, J., Walsh, C.T., Silverstein, S.C., (1974). Determination of the absolute number of *Escherichia coli* membrane vesicles that catalyze active transport. *PNAS* **71**, 5032–5036.
46. Chae, P.S., Rasmussen, S.G., Rana, R.R., Gotfryd, K., Chandra, R., Goren, M.A., Kruse, A.C., Nurva, S., et al., (2010). Maltose-neopentyl glycol (MNG) amphiphiles for solubilization, stabilization and crystallization of membrane proteins. *Nature Methods* **7**, 1003–1008.
47. Ritchie, T.K., Grinkova, Y.V., Bayburt, T.H., Denisov, I.G., Zolnerciks, J.K., Atkins, W.M., Sligar, S.G., (2009). Chapter 11 – Reconstitution of membrane proteins in phospholipid bilayer nanodiscs. *Methods Enzymol.* **464**, 211–231.
48. Zoghbi, M.E., Cooper, R.S., Altenberg, G.A., (2016). The Lipid Bilayer Modulates the Structure and Function of an ATP-binding Cassette Exporter. *J. Biol. Chem.* **291**, 4453–4461.
49. Jo, S., Kim, T., Iyer, V.G., Im, W., (2008). CHARMM-GUI: A web-based graphical user interface for CHARMM. *J. Comput. Chem.* **29**, 1859–1865.
50. Beglov, D., Roux, B., (1994). Finite representation of an infinite bulk system: Solvent boundary potential for computer simulations. *J. Chem. Phys.* **100**, 9050–9063.
51. Klauda, J.B., Venable, R.M., Freites, J.A., O'Connor, J.W., Tobias, D.J., Mondragon-Ramirez, C., Vorobyov, I., MacKerell, A.D., et al., (2010). Update of the CHARMM All-Atom Additive Force Field for Lipids: Validation on Six Lipid Types. *J. Phys. Chem. B* **114**, 7830–7843.
52. Best, R.B., Zhu, X., Shim, J., Lopes, P.E.M., Mittal, J., Feig, M., MacKerell, A.D., (2012). Optimization of the

Additive CHARMM All-Atom Protein Force Field Targeting Improved Sampling of the Backbone phi, psi and Side-Chain chi(1) and chi(2) Dihedral Angles. *J. Chem. Theory Comput.* **8**, 3257–3273.

53. Guvench, O., Hatcher, E., Venable, R.M., Pastor, R.W., MacKerell, A.D., (2009). CHARMM Additive All-Atom Force Field for Glycosidic Linkages between Hexopyranoses. *J. Chem. Theory Comput.* **5**, 2353–2370.
54. Darden, T., York, D., Pedersen, L., (1993). Particle mesh Ewald: An Ṅslog(N) method for Ewald sums in large systems. *J. Chem. Phys.* **98**, 10089–10092.
55. Jorgensen, W.L., Chandrasekhar, J., Madura, J.D., Impey, R.W., Klein, M.L., (1983). Comparison of Simple Potential Functions for Simulating Liquid Water. *J. Chem. Phys.* **79**, 926–935.
56. Eastman, P., Friedrichs, M.S., Chodera, J.D., Radmer, R. J., Bruns, C.M., Ku, J.P., Beauchamp, K.A., Lane, T.J., et al., (2013). OpenMM 4: A Reusable, Extensible, Hardware Independent Library for High Performance Molecular Simulation. *J. Chem. Theo. Comp.* **9**, 461–469.